



23 versy since the first detection by Smylie (1992) of a triplet of frequencies  
24 that he attributed to the Slichter modes. This detection has been sup-  
25 ported by Courtier et al. (2000) and Pagiatakis et al. (2007) but has not  
26 been confirmed by other authors (Hinderer et al., 1995; Jensen et al., 1995;  
27 Rosat et al., 2006; Guo et al., 2007). Also, it motivated additional theoretical  
28 studies (Crossley, 1992; Rochester and Peng, 1993; Rieutord, 2002; Rogister,  
29 2003). The search for the Slichter modes was invigorated by the develop-  
30 ment of worldwide data recorded by superconducting gravimeters (SGs) of  
31 the Global Geodynamics Project (Hinderer and Crossley, 2000). Thanks to  
32 their long-time stability and low noise level, these relative gravimeters are the  
33 most suitable instruments to detect the small signals that would be expected  
34 from the Slichter modes (Hinderer et al., 1995; Rosat et al., 2003, 2004).

35 The theory is now better understood and computation predicts eigen-  
36 periods between 4 and 6 h (Rogister, 2003) for the seismological reference  
37 PREM (Dziewonski and Anderson, 1981) Earth model. A more recent study  
38 by Grinfeld and Wisdom (2010) states that the period could be much shorter  
39 because of the kinetics of phase transformations at the inner-core boundary  
40 (ICB).

41 The observation of the Slichter modes is fundamental because, the restor-  
42 ing force being Archimedean, their periods are directly related to the density  
43 jump at the ICB. This parameter is still poorly known: by analyzing seismic  
44 PKiKP/PcP phases, Koper and Pyle (2004) found that it should be smaller  
45 than  $450 \text{ kg/m}^3$ , later increased to  $520 \text{ kg/m}^3$  (Koper and Dombrovskaya,  
46 2005), whereas Masters and Gubbins (2003) obtained  $820 \pm 180 \text{ kg/m}^3$  from  
47 normal modes observation. Tkalčić et al. (2009) have shown that the un-

48 certainties associated with the seismic noise might partially explain such  
49 discrepancies for the estimates of the ICB density contrast. Gubbins et al.  
50 (2008) have proposed a model with a large overall density jump between the  
51 inner and outer cores of  $800 \text{ kg/m}^3$  and a sharp density jump of  $600 \text{ kg/m}^3$   
52 at the ICB itself. Such a model satisfies both the constraints set by powering  
53 the geodynamo with a reasonable heat flux from the core, and PKP travel-  
54 times and normal mode frequencies. The value of the density jump at ICB  
55 for the PREM model is  $600 \text{ kg/m}^3$ .

56 This paper aims at evaluating the possible amplitude of the Slichter modes  
57 for various types of excitation sources.

58 The seismic excitation has been previously studied by Smith (1976),  
59 Crossley (1992) and Rosat (2007). They have shown that the best natu-  
60 ral focal mechanism to excite the Slichter mode is a vertical dip-slip source.  
61 The largest magnitude event in the past was the 1960 Chile earthquake with  
62 a magnitude  $M_w = 9.6$  for the main shock. A foreshock occurred with a mag-  
63 nitude of 9.5 (Kanamori and Cipar, 1974). The combination of both events  
64 leads to a seismic source of magnitude  $M_w = 9.8$  which would be enough to  
65 excite the Slichter modes to the nanoGal level. However, at such frequen-  
66 cies, the noise levels of SGs are of several nGal, even for the quietest sites  
67 (Rosat and Hinderer, 2011). Earthquakes are therefore not the most suitable  
68 source to excite the Slichter modes to a level sufficient for the SGs to detect  
69 the induced surface gravity effect.

70 Surficial pressure flow acting in the core has been considered by Greff-Lefftz and Legros  
71 (2007) as a possible excitation source. In this work, we reconsider the pres-  
72 sure flow acting in the core using a Green function formalism for a non-

73 rotating anelastic PREM Earth model. Then, we investigate the surface  
 74 load and meteoroid impact as possible sources of excitation of the Slichter  
 75 modes.

## 76 2. Green function formalism

77 We consider a spherical non-rotating anelastic Earth model. The dis-  
 78 placement  $\mathbf{u}$  at a point  $\mathbf{r}$  and time  $t$  produced by any body force density  $\mathbf{f}$   
 79 acting in volume  $V$  and surface force density  $\mathbf{t}$  acting upon surface  $S$  can  
 80 be written as a convolution of the impulse response  $G$  with the entire past  
 81 history of the forces  $\mathbf{f}$  and  $\mathbf{t}$  (Dahlen and Tromp, 1998):

$$\mathbf{u}(\mathbf{r}, t) = \int_{-\infty}^t \int_V G(\mathbf{r}, \mathbf{r}'; t - t') \mathbf{f}(\mathbf{r}', t') dV' dt' + \int_{-\infty}^t \int_S G(\mathbf{r}, \mathbf{r}'; t - t') \mathbf{t}(\mathbf{r}', t') d\Sigma' dt', \quad (1)$$

82 where  $\mathbf{r}'$  is the integrated position vector. This relation is inferred from  
 83 Betti's reciprocity relation in seismology (Aki and Richards, 1980). Seismic  
 84 Green's tensor  $G$  of a non-rotating anelastic Earth is given in terms of the  
 85 normal-mode complex frequencies  $\nu_k = \omega_k(1 + \frac{i}{2Q_k})$  and eigenfunctions  $\mathbf{s}_k$  by

$$G(\mathbf{r}, \mathbf{r}'; t) = \Re \sum_k (i\nu_k)^{-1} \mathbf{s}_k(\mathbf{r}) \mathbf{s}_k(\mathbf{r}') e^{i\nu_k t} H(t), \quad (2)$$

86 where  $\Re$  denotes the real part of the complex expression and  $H(t)$  is the  
 87 Heaviside function.

88 Tromp and Mitrovica (1999) have generalized Betti's reciprocity relation  
 89 to a representation theorem suited for surface-load problems, so that the  
 90 displacement  $\mathbf{u}$  due to a surface load  $\sigma$  located at  $\mathbf{r}'$  is given by

$$\mathbf{u}(\mathbf{r}, t) = \int_{-\infty}^t \int_S \sigma(\mathbf{r}', t') \mathbf{\Gamma}(\mathbf{r}, \mathbf{r}'; t - t') d\Sigma' dt', \quad (3)$$

91 where  $\mathbf{\Gamma}$  is the surface-load Green's vector defined by

$$\mathbf{\Gamma}(\mathbf{r}, \mathbf{r}'; t) = -[G(\mathbf{r}, \mathbf{r}'; t) \cdot \nabla' \Phi(\mathbf{r}') + \mathbf{g}(\mathbf{r}, \mathbf{r}'; t)], \quad (4)$$

92  $\nabla'$  is the gradient with respect to  $\mathbf{r}'$ ,  $\Phi$  is the unperturbed gravitational  
93 potential, and  $\mathbf{g}$  is

$$\mathbf{g}(\mathbf{r}, \mathbf{r}'; t) = \Re \sum_k (i\nu_k)^{-1} \phi_k(\mathbf{r}) \mathbf{s}_k(\mathbf{r}') e^{i\nu_k t} H(t), \quad (5)$$

94  $\phi_k$  denoting the perturbation of the gravitational potential associated with  
95 the normal mode  $\{\mathbf{s}_k, \phi_k\}$ . Green's tensor  $\{G, \mathbf{g}\}$  represents the complete  
96 point-source response.

97 A spheroidal mode of harmonic degree  $l$  and order  $m$  and radial overtone  
98 number  $n$  can be decomposed into three components in spherical coordinates:

$${}_n \mathbf{s}_l^m(\mathbf{r}) = {}_n U_l^m(r) Y_l^m(\theta, \phi) \hat{\mathbf{r}} + k^{-1} {}_n V_l^m(r) \frac{\partial Y_l^m}{\partial \theta} \hat{\theta} + k^{-1} {}_n V_l^m(r) \frac{1}{\sin \theta} \frac{\partial Y_l^m}{\partial \phi} \hat{\phi}, \quad (6)$$

99 where  $Y_l^m(\theta, \phi)$  are the real spherical harmonics of degree  $l$  and order  $m$   
100 (Dahlen and Tromp, 1998),  $k = \sqrt{l(l+1)}$  and  $\hat{\mathbf{r}}$ ,  $\hat{\theta}$  and  $\hat{\phi}$  are the usual  
101 unit vectors of the spherical coordinates. The associated perturbation of the  
102 gravitational potential has the form

$${}_n \phi_l^m(\mathbf{r}) = {}_n P_l^m(r) Y_l^m(\theta, \phi). \quad (7)$$

103 The eigenfunctions  ${}_n U_l^m(r)$ ,  ${}_n V_l^m(r)$  and  ${}_n P_l^m(r)$  are functions of the radius  
104 only. Because the model is non-rotating and spherically symmetric, the  $2l+1$   
105 eigenfrequencies for each fixed  $l$  and  $n$  are degenerate into a single eigenfre-  
106 quency that we can therefore denote by  ${}_n \nu_l$ . The summation over  $k$  in Eqs  
107 (2) and (5) is actually a triple summation over  $l$ ,  $m$  and  $n$ . Since the eigen-  
108 frequencies do not depend on  $m$ , the summation over  $m$  can be performed

109 using the addition theorem for surface spherical harmonics, with the result  
 110 [Dahlen and Tromp (1998), Eqs 10.28 and 10.34]:

$$\begin{aligned}
 G(\mathbf{r}, \mathbf{r}'; t) = \Re \sum_n \sum_l \frac{2l+1}{4\pi} \frac{e^{i_n \nu_l t}}{i_n \nu_l} & \\
 \{ {}_n U_l(r) {}_n U_l(r') \hat{\mathbf{r}} \hat{\mathbf{r}}' P_{l0} & \\
 + k^{-1} [ {}_n U_l(r) {}_n V_l(r') \hat{\mathbf{r}} \hat{\Theta}' - {}_n V_l(r) {}_n U_l(r') \hat{\Theta} \hat{\mathbf{r}}' ] P_{l1} & \\
 + \frac{1}{2} k^{-2} [ {}_n V_l(r) {}_n V_l(r') \hat{\Theta} \hat{\Theta}' ] (k^2 P_{l0} - P_{l2}) & \\
 + k^{-2} [ {}_n V_l(r) {}_n V_l(r') \hat{\Phi} \hat{\Phi}' ] (\sin \Theta)^{-1} P_{l1} \}, & \quad (8)
 \end{aligned}$$

111 where  $\hat{\Phi} = \hat{\mathbf{r}} \times \hat{\Theta}$  and  $\Theta$  is the angular distance between the receiver at  $\hat{\mathbf{r}}$   
 112 and the point source at  $\hat{\mathbf{r}}'$ :

$$\cos \Theta = \hat{\mathbf{r}} \cdot \hat{\mathbf{r}}' = \cos \theta \cos \theta' + \sin \theta \sin \theta' \cos(\phi - \phi'). \quad (9)$$

113 The Slichter mode is the spheroidal mode of harmonic degree one and  
 114 radial overtone number one. For a non-rotating spherical model, the three  
 115 Slichter frequencies are degenerate into a single eigenfrequency. As

$$P_{10}(\cos \Theta) = \cos \Theta \quad (10)$$

116 and

$$P_{11}(\cos \Theta) = \sin \Theta, \quad (11)$$

117 the term for which  $l = 1$  and  $n = 1$  in Eq. (8) writes:

$$\begin{aligned}
 {}_1 G_1(\mathbf{r}, \mathbf{r}'; t) = \frac{3}{4\pi} \Re \{ & \frac{e^{i\nu}}{i\nu} [U(r)U(r') \hat{\mathbf{r}} \hat{\mathbf{r}}' \cos \Theta \\
 + \frac{1}{\sqrt{2}} (U(r)V(r') \hat{\mathbf{r}} \hat{\Theta}' - V(r)U(r') \hat{\Theta} \hat{\mathbf{r}}') \sin \Theta & \\
 + \frac{1}{2} V(r)V(r') \hat{\Theta} \hat{\Theta}' \cos \Theta + \frac{1}{2} V(r)V(r') \hat{\Phi} \hat{\Phi}' \} & \quad (12)
 \end{aligned}$$

118 being understood that  $\nu = {}_1\nu_1$ ,  $U = {}_1U_1$ ,  $V = {}_1V_1$  and  $P = {}_1P_1$ . For PREM,  
119 the Slichter eigenperiod is 5.42 h (Rogister, 2003) and the eigenfunctions  $U$ ,  
120  $V$  and  $P$  are plotted in Fig. A.1.

121 The damping rate depends on the dissipation processes involved. A sum-  
122 mary of plausible dissipation processes is given by Greff-Lefftz and Legros  
123 (2007); Guo et al. (2007); Rosat et al. (2007). The role of the outer core vis-  
124 cosity has been studied by Smylie and McMillan (2000) and Rieutord (2002),  
125 the effect of a mushy zone at the ICB, by Peng (1997), the influence of the  
126 magnetic field, by Buffett and Goertz (1995) and the anelastic dissipation  
127 for the core modes, by Crossley et al. (1992). Such studies have revealed  
128 that it is unlikely that the damping factor of the Slichter mode be less than  
129 2000, corresponding to a damping time of 144 days. In this case, the induced  
130 surface gravity perturbation should be more easily detectable by SGs. We  
131 assume, in the following, a quality factor of 2000.

132 Using the Green function formalism, we can compute the excitation of  
133 the Slichter mode by any body or surface forces.

### 134 **3. Excitation by fluid core pressure**

135 Observational evidence for motions in the core comes from core-sensitive  
136 seismic modes, which have periods smaller than one hour, the free core nu-  
137 tation, which is a rotational mode of nearly-diurnal period, and variations of  
138 the magnetic field that can be related to motions in the core with timescales  
139 larger than one year. Therefore, the dynamics of the fluid core at the Slichter  
140 frequencies lacks observational evidence. Theoretical results suggest that, at  
141 timescales smaller than one day and outside the seismic band, plausible mo-

142 tions are to be searched for in the turbulent convection or in the spectrum  
143 of the core.

144 An account of small-scale turbulence driven by convection is given by  
145 Loper (2007). The timescale may be less than one day but, because of  
146 the small characteristic length-scales, turbulence is unlikely to excite the  
147 translation of the whole inner core.

148 Valette (1989a,b) has shown that the inertia-gravity spectrum of an in-  
149 viscid liquid core is continuous and set bounds on it. The bounds de-  
150 pend on both the speed of rotation and squared Brunt-Väisälä frequency.  
151 Rogister and Valette (2009) and Rogister (2010) have suggested that the ro-  
152 tational modes might be influenced by the continuous spectrum in which  
153 they are embedded. In particular, the nearly-diurnal free inner core nutation  
154 and long-period inner core wobble might be double or even multiple and have  
155 energy in the liquid core. Pending on the value of the squared Brunt-Väisälä  
156 frequency in the outer core, the Slichter modes could also be embedded in  
157 the continuous spectrum. Similarly to what has been found for the two ro-  
158 tational modes of the inner core, significant motion and pressure variation  
159 in the liquid core could accompany the Slichter modes. Although a Slichter  
160 mode with its associated motion in the liquid core should then be considered  
161 as a single normal mode, we can for simplicity assume that the pressure vari-  
162 ations in the liquid core excite the translational motions of the inner core.  
163 This is somewhat the opposite of what Buffett (2010) did to investigate the  
164 attenuation of the free inner core nutation: he assumed that the tilt of the  
165 inner core generates shear layers in the outer core where Ohmic and viscous  
166 dissipation occur.



167 As Greff-Lefftz and Legros (2007), we will assume that the pressure at  
 168 the CMB takes the following analytical form:

$$P^c(\theta, \phi, t) = P_0^c(\theta, \phi)e^{-\left(\frac{t-T_0}{\tau}\right)^2}, \quad (13)$$

169 where  $T_0$  is the starting time of application of the pressure,  $\tau$  is the time  
 170 duration of the pressure source and  $P_0^c(\theta, \phi)$  includes three terms of harmonic  
 171 degree 1:

$$P_0^c(\theta, \phi) = P_{10}^c \cos \theta + (P_{11}^c \cos \phi + \tilde{P}_{11}^c \sin \phi) \sin \theta. \quad (14)$$

172 According to Okubo and Endo (1986) and Greff-Lefftz and Legros (2007),  
 173 the total force exerted at the core boundaries must vanish for the centre of  
 174 mass to be kept fixed. This translates into the so-called Consistency Relation  
 175 (Farrell, 1972) and imposes a relation between the pressures  $P^c$  and  $P^{ic}$  at  
 176 the CMB and ICB, respectively:

$$P^{ic} = \frac{r_c^2}{r_{ic}^2} P^c. \quad (15)$$

177 Greff-Lefftz and Legros (2007) analytically solved the equations of the  
 178 elasto-gravitational deformation (Alterman et al. , 1959) for a simple Earth  
 179 model made up of three homogeneous incompressible layers and investigated  
 180 the excitation of the Slichter mode by a pressure acting at the outer core  
 181 boundaries. In this section, we consider the same simple excitation sources  
 182 to test the Green function approach for PREM, which is a more realistic  
 183 Earth model. We compute the displacement  $\mathbf{u}$  by means of Eqs (1) and (12).  
 184 As we are mainly interested in the surface gravity effect, we only need the  
 185 radial component of the displacement:

$$u_r(r, \theta, \phi, t) = \frac{3}{4\pi} \Re \left\{ \frac{U(r)}{i\nu} \int_{-\infty}^t e^{i\nu(t-t')} e^{-\left[\frac{t'-T_0}{\tau}\right]^2} dt' \right\}$$

$$[U(r_c) \int_{\text{CMB}} \cos \Theta (P_{10}^c \cos \theta' + (P_{11}^c \cos \phi' + \tilde{P}_{11}^c \sin \phi') \sin \theta') d\Sigma' - U(r_{ic}) \int_{\text{ICB}} \cos \Theta (P_{10}^{ic} \cos \theta' + (P_{11}^{ic} \cos \phi' + \tilde{P}_{11}^{ic} \sin \phi') \sin \theta') d\Sigma'] \quad (16)$$

186 At the CMB,  $d\Sigma' = r_c^2 \sin \theta' d\theta' d\phi'$  and, at the ICB,  $d\Sigma' = r_{ic}^2 \sin \theta' d\theta' d\phi'$ .

187 Taking Eqs (9) and (15) into account, the integration over  $\theta'$  and  $\phi'$  gives:

$$u_r(r, \theta, \phi, t) = \Re \left\{ \frac{r_c^2 U(r)}{i\nu} [U(r_c) - U(r_{ic})] \int_{-\infty}^t e^{i\nu(t-t')} e^{-[\frac{t'-T_0}{\tau}]^2} dt' (P_{10}^c \cos \theta + P_{11}^c \sin \theta \cos \phi + \tilde{P}_{11}^c \sin \theta \sin \phi) \right\} \quad (17)$$

188 The integral

$$I(t) = \int_{-\infty}^t e^{i\nu(t-t')} e^{-[\frac{t'-T_0}{\tau}]^2} dt' \quad (18)$$

189 is calculated in the Appendix. It gives

$$I(t) = \frac{\sqrt{\pi}}{2} \tau e^{i\nu(t-T_0)} e^{-\nu^2 \tau^2 / 4} [1 + \operatorname{erf}(\frac{t-T_0}{\tau} + i\frac{\nu\tau}{2})], \quad (19)$$

190 where  $\operatorname{erf}$  denotes the error function. The radial displacement then becomes:

$$u_r(r, \theta, \phi, t) = -\frac{r_c^2 U(r)}{\omega(1 + \frac{1}{4Q^2})} [U(r_c) - U(r_{ic})] \left[ \frac{\Re\{I(t)\}}{2Q} - \Im\{I(t)\} \right] (P_{10}^c \cos \theta + P_{11}^c \sin \theta \cos \phi + \tilde{P}_{11}^c \sin \theta \sin \phi), \quad (20)$$

191 where  $\Re\{ \}$  and  $\Im\{ \}$  respectively denote the real and imaginary parts of the  
192 expression between brackets.

193 The degree- $l$  gravity variation measured by a gravimeter at the surface of  
194 the Earth  $r_s$  is the sum of three terms: the free-air gravity variation owing  
195 to the displacement of the ground in the surrounding unperturbed gravity  
196 field  $g_0$

$$g_{\text{free}} = (-4\pi G \bar{\rho} + \frac{2}{r_s} g_0) U(r_s), \quad (21)$$

197 the inertial acceleration of the ground

$$g_{\text{in}} = -\omega_l^2 U(r_s) \quad (22)$$

198 and the perturbation of the gravitational attraction

$$g_{\text{pot}} = 4\pi G \bar{\rho} U(r_s) + \frac{2}{r_s} P(r_s). \quad (23)$$

199 In these expressions,  $\bar{\rho}$  is the mean density of the Earth.

200 The degree-1 gravity variation measured by a gravimeter is therefore

$$\begin{aligned} \Delta g(\theta, \phi, t) = & \frac{r_c^2}{\omega(1 + \frac{1}{4Q^2})} [U(r_c) - U(r_{ic})] \\ & [P_{10}^c \cos \theta + P_{11}^c \sin \theta \cos \phi + \tilde{P}_{11}^c \sin \theta \sin \phi] \\ & [\frac{\Re\{I(t)\}}{2Q} - \Im\{I(t)\}] [-\omega^2 U(r_s) + \frac{2}{r_s} g_0 U(r_s) + \frac{2}{r_s} P(r_s)] \end{aligned} \quad (24)$$

201 We consider a zonal pressure  $P_{10}^c = 150$  Pa and compute the induced  
 202 geocentre motion, inner-core translation and surface gravity perturbation for  
 203 both  $\tau = 1.5$  h and 15 h (Fig. A.2). As the centre of mass is fixed, the geocen-  
 204 tre motion, which is the displacement of the figure centre with respect to the  
 205 centre of mass, corresponds to the surface displacement (Greff-Lefftz and Legros,  
 206 1997).

207 For  $P_{10}^c$  varying from 0 to 1000 Pa and  $\tau$  ranging from 0.1 and 10 h, we  
 208 compute a 2D-map (Fig. A.3) of the surface gravity perturbation when the  
 209 exciting pressure has vanished (i.e.  $t > T_0 + \tau$ ).

210 Our results for the PREM model show excitation amplitudes larger by  
 211 70 % than the amplitudes computed by Greff-Lefftz and Legros (2007), who  
 212 used a very simple model made up of three incompressible homogeneous  
 213 layers with a solid inner core, a liquid outer core and a rigid mantle. If

214 we consider such a 3-layer model with the average densities of the PREM  
215 inner core, outer core and mantle, we obtain a period of 3.09 h for the  
216 Slichter mode and excitation amplitudes in close agreement with the values  
217 of Greff-Lefftz and Legros (2007). They do not provide numerical details for  
218 the structure of their model but mention that its Slichter period is 3.08 h,  
219 which is almost equal to the Slichter period of our 3-layer model. Therefore,  
220 the Green function formalism we have adopted gives the same result as the  
221 analytical solution for the degree-1 deformation of a simple 3-layer model  
222 obtained by Greff-Lefftz and Legros (2007).

223 The difference between the excitation amplitudes we obtain for PREM  
224 and the amplitudes computed by Greff-Lefftz and Legros (2007) comes from  
225 the different Earth models. The elasticity of the mantle and inner core, the  
226 compressibility of the outer core and the density jump at the ICB all come  
227 into play. Greff-Lefftz and Legros (2007) mention that the elasticity of the  
228 mantle perturbs the solutions by 30 %, without any further specifications.  
229 We have checked that, by making the outer core of our simple 3-layer model  
230 compressible, with a P-wave velocity of 11083 m/s, the excitation amplitude  
231 of the Slichter mode is decreased by 40 % with respect to the incompressible  
232 model. The influence of the compressibility and stratification of the core on  
233 the Slichter mode was also investigated by Rogister (2003).

234 The perturbation of the surface gravity field is the largest when  $\tau$  is  
235 smaller than half the Slichter eigenperiod. When  $\tau$  is one fourth of the  
236 Slichter period, a 10 Pa pressure acting at the CMB, which by Eq. (15)  
237 imposes a 81 Pa pressure at the ICB, is enough to induce a 10 nGal (0.1  
238 nm/s<sup>2</sup>) surface gravity perturbation, which should be detectable by SGs.

239 **4. Excitation by a surface load**

240 A degree- $l$  surficial mass distribution  $\sigma^s$  at the surface  $r_s$  exerts forces  
 241 over the Earth in two ways. First, at the interface between the Earth and  
 242 the load  $\sigma^s$ , the static contact forces give rise to a degree- $l$  pressure

$$P^s = g_0 \sigma^s. \quad (25)$$

243 Second, the gravitational attraction of the load  $\sigma^s$  over the entire Earth is  
 244 described by a degree- $l$  potential

$$\phi = \frac{4\pi G}{2l+1} \sigma^s r_s \begin{cases} \left(\frac{r}{r_s}\right)^l & \text{if } r \leq r_s \\ \left(\frac{r_s}{r}\right)^l & \text{if } r > r_s \end{cases} \quad (26)$$

245 Atmospheric pressure models are sampled at 3 h at best. So instead of  
 246 using actual data, we write the surface density load in the analytical form:

$$\sigma^s(\theta, \phi, t) = \sigma_0^s(\theta, \phi) e^{-\left[\frac{t-T_0}{\tau}\right]^2}, \quad (27)$$

247 which is the same as the expression used for the fluid core pressure in Section  
 248 3. The degree-one load  $\sigma_0^s$ , like  $P_0^c$ , contains three terms:

$$\sigma_0^s(\theta, \phi) = \sigma_{10} \cos \theta + (\sigma_{11} \cos \phi + \tilde{\sigma}_{11} \sin \phi) \sin \theta. \quad (28)$$

249 After integration of Eq. (3) over the whole surface, the radial displace-  
 250 ment is given by:

$$u_r(r, \theta, \phi, t) = \frac{r_s^2 U(r)}{\omega \left(1 + \frac{1}{4Q^2}\right)} [U(r_s) g_0 + P(r_s)] \left[ \frac{\Re\{I(t)\}}{2Q} - \Im\{I(t)\} \right] \\ [\sigma_{10} \cos \theta + \sigma_{11} \sin \theta \cos \phi + \tilde{\sigma}_{11} \sin \theta \sin \phi], \quad (29)$$

251 and the perturbation of the surface gravity is

$$\begin{aligned}
\Delta g(t) = & \frac{r_s^2}{\omega(1 + \frac{1}{4Q^2})} [U(r_s)g_0 + P(r_s)] [\frac{\Re\{I(t)\}}{2Q} - \Im\{I(t)\}] \\
& [\sigma_{10} \cos \theta + \sigma_{11} \sin \theta \cos \phi + \tilde{\sigma}_{11} \sin \theta \sin \phi] \\
& [-\omega^2 U(r_s) + \frac{2}{r_s} g_0 U(r_s) + \frac{2}{r_s} P(r_s)] \tag{30}
\end{aligned}$$

252 We use a zonal surface load pressure of 1000 Pa (the surface mass density  
253 is then  $\sigma_{10} = P_{10}/g_0$ ) and we compute the induced geocentre motion, the  
254 inner-core translation and the surface gravity perturbation for two excitation  
255 time-scales (1.5 h and 15 h) (Fig. A.4). When applying a surface load of  
256 1000 Pa during  $2\tau = 3$  h, the induced surface gravity perturbation has an  
257 amplitude of 5 nGal ( $0.05 \text{ nm/s}^2$ ) corresponding to an inner-core translation  
258 of 15 mm and a geocentre motion in the opposite direction with an amplitude  
259 of 0.015 mm. When the excitation time-scale (15 h) is larger than the Slichter  
260 period, the excitation amplitude is smaller.

261 We also plot the surface gravity perturbation associated to the Slichter  
262 mode excited by a surface load for different excitation time-scales and various  
263 zonal pressure amplitudes in Fig. A.5. The conclusion is similar to the one  
264 for an internal pressure flow, except that the surface gravity variations are  
265 about 300 times smaller.

266 In this section, we have estimated the effect of a surface load on the  
267 Slichter mode. Another source that, intuitively, could make the inner core  
268 oscillate is a shock at the surface. Hence, in the next section, we study the  
269 excitation by an object impact on the Earth's surface.

## 270 **5. Excitation by an object impact**

271 Stellar objects, such as asteroids or comets, are dragged by the Earth's  
272 atmosphere and reach the Earth's surface at relatively modest velocities,  
273 typically a few tens of km/s. The released energy is comparable to nuclear  
274 explosions (according to Table 6 of Collins et al. (2005), from 3.2 to 3.9 10<sup>8</sup>  
275 megatons of TNT, where 1 Mt = 4.2 10<sup>15</sup> J). The collisions between the  
276 Earth and the largest meteoroids, with diameters from hundreds of meters  
277 to several kilometers, blast out the impacting objects, create wide craters,  
278 generally twenty times larger than the diameter of the meteoroids, and melt  
279 terrestrial rocks. Fortunately, such collisions are rare events: statistically,  
280 a 100 to 200 m meteoroid hits the Earth every 1000 years, a 500 to 800 m  
281 meteoroid every 30000 years, and a 5 km meteoroid every 40 millions years.

282 We believe it is reasonable to assume that both the mass and linear mo-  
283 mentum of the impacting object are negligible with respect to the Earth's  
284 mass and linear momentum, so the orbit of the Earth is not disturbed. Be-  
285 sides, the rotation period and tilt of the rotation axis of the Earth could  
286 be changed by the impact if the angular momentum of the object is large  
287 enough. We, however, consider impactors for which the angular momen-  
288 tum is at least one hundred times smaller than the Earth's; the change of  
289 the Earth's angular momentum is therefore negligible. The major known  
290 meteoroid impacts had such characteristics (Table A.1).

291 Consequently, we reduce the extraterrestrial impact issue to the com-  
292 putation of the equivalent seismic magnitude corresponding to the released  
293 energy. The computation proposed here is based on the equations and drastic  
294 simplifications used by Collins et al. (2005), which are summarized below.

295 When an object enters the Earth's atmosphere, it loses its kinetic energy  
 296 through deceleration and ablation. The rate of change of the velocity  $v$  is  
 297 given by the drag equation (Collins et al., 2005; Melosh, 1989):

$$\frac{dv}{dt} = -\frac{3\rho z C_D}{4\rho_i L_0} v^2, \quad (31)$$

298 where  $z$  is the altitude,  $C_D$  is the drag coefficient, taken equal to 2, and  $\rho_i$   
 299 and  $L_0$  are, respectively, the impactor density and diameter. By assuming  
 300 an exponential atmosphere,

$$\rho(z) = \rho_0 e^{-z/H}, \quad (32)$$

301 where  $H = 8$  km is the scale height and  $\rho_0 = 1$  kg/m<sup>3</sup>, the velocity of the  
 302 impactor as a function of altitude is given by:

$$v(z) = v_0 \exp\left(-\frac{3\rho(z)C_D H}{4\rho_i L_0 \sin \alpha}\right), \quad (33)$$

303 where  $\alpha$  is the entry angle and  $v_0$ , the velocity at the top of the atmosphere.  
 304 On its trajectory down to the ground, the impactor goes through the in-  
 305 creasing atmospheric pressure and, possibly, breaks up. Collins et al. (2005)  
 306 have established an empirical strength-density relation to estimate the yield  
 307 strength  $Y_i$  (in Pa)

$$\log_{10} Y_i = 2.107 + 0.0624\sqrt{\rho_i} \quad (34)$$

308 and give an approximate expression for the altitude of breakup  $z^*$ :

$$z^* \approx -H\left[\ln\left(\frac{Y_i}{\rho_0 v_i^2}\right) + 1.308 - 0.314I_f - 1.303\sqrt{1 - I_f}\right], \quad (35)$$

309 where

$$I_f = 4.07 \frac{C_D H Y_i}{\rho_i L_0 v_i^2 \sin \alpha}, \quad (36)$$



310 and  $v_i$  is the impactor velocity at the surface.

311 Equation (35) holds provided that  $I_f < 1$ . Otherwise, and more rarely,  
 312 the object does not break up and the velocity at the impact is given by  
 313 Equation (33).

314 Following Collins et al. (2005), we use the approximative pancake model  
 315 (Chyba et al., 1993; Melosh, 1981) to describe the disintegration of the me-  
 316 teoroid. Let us denote by  $z_b$  the airburst altitude, which is the altitude of  
 317 complete dispersion of the fragments. According to the simplifying assump-  
 318 tions of the pancake model,  $z_b$  is given by

$$z_b = z^* - 2H \ln\left(1 + \frac{\ell}{2H} \sqrt{f_p^2 - 1}\right), \quad (37)$$

319 where  $\ell$  is the dispersion length scale:

$$\ell = L_0 \sin \alpha \sqrt{\frac{\rho_i}{C_D \rho(z^*)}} \quad (38)$$

320 and the pancake factor  $f_p$  is between 2 and 10. We shall adopt Collins et al.  
 321 (2005)'s value of 7. If  $z_b > 0$ , the airburst occurs in the atmosphere, there is  
 322 neither impact nor associated seismic event. If  $z_b \leq 0$ , the fragments are not  
 323 dispersed when they collide with the ground and the impact velocity is:

$$v_{zr} = v(z^*) \exp \left\{ \left( -\frac{3}{4} \frac{C_D \rho(z^*)}{\rho_i L_0^3 \sin \alpha} \frac{H^3 L_0^2}{3\ell^2} \left( 32 + \left( \frac{\ell}{H} \right)^2 e^{z^*/H} \right. \right. \right. \\ \left. \left. \left. + 6e^{2z^*/H} - 16e^{3z^*/2H} - 3\left( \frac{\ell}{H} \right)^2 \right) \right\} \quad (39)$$

324 The remaining kinetic energy at the moment of impact is

$$E_{cr} = \frac{\pi}{12} \rho_i L_0^3 v_{zr}^2. \quad (40)$$

325 After the impact, a fraction  $k_s$  of  $E_{cr}$  is radiated as seismic waves. Exper-  
 326 imental data (Schultz and Gault, 1975) provide  $k_s \in [10^{-5}, 10^{-3}]$ . We will

327 take  $k_s = 10^{-4}$ . The seismic moment being given by

$$M_0 = 2 \frac{\mu}{\Delta\sigma_S} k_s E_{cr}, \quad (41)$$

328 where the stress release  $\Delta\sigma_S \approx 3$  MPa and the rigidity  $\mu = 30$  GPa, the  
329 seismic magnitude is then:

$$M_w = \frac{2}{3} \log_{10}(M_0) - 10.73 \quad (42)$$

330 with  $M_0$  in dyn.cm ( $1 \text{ dyn.cm} = 10^{-7} \text{ N/m}$ ).

331 We compute the magnitude  $M_w$  for the different meteoroid impacts of  
332 Table A.1 and, in the same table, report the surface gravity perturbation  
333 associated with the translational excitation of the inner core. Note that the  
334 source is represented in terms of moment tensor by three orthogonal force  
335 couples (spherically symmetric explosion) and not as a vertical force. Indeed,  
336 the shock pressure would reach hundreds of gigapascals and the impact en-  
337 ergy would vaporize the rocks and cause a spherically symmetric explosion,  
338 as observed from the spherical shape of known craters.

339 For the biggest meteoroid, the surface excitation amplitude of the Slichter  
340 mode is  $0.0067 \text{ nm/s}^2$ , which is less than the detection threshold of  $1 \text{ nGal}$   
341 ( $= 0.01 \text{ nm/s}^2$ ). To determine what kind of impact would be necessary to  
342 excite sufficiently the Slichter mode so that it is detectable in surface gravity  
343 data, we compute the magnitude  $M_w$  and gravity perturbation  $\Delta g$  for various  
344 ranges of density  $\rho_i$ , velocity  $v_0$ , diameter  $L_0$  of the object and for seismic  
345 efficiency  $k_s$  varying between  $10^{-5}$  and  $10^{-2}$ . The resulting maps are plotted  
346 in Fig.A.6. The shaded areas correspond to  $M_w$  larger than 9.7, which is the  
347 magnitude required for the surface gravity effect to reach the nGal detection  
348 threshold for a surficial explosive moment source (Fig. A.7).

349 We see from Fig.A.6 that to produce a seismic event of magnitude larger  
350 than 9.7, the size, density or velocity of the impacting object should have  
351 unrealistic huge values. However, the value of the seismic efficiency  $k_s$  has  
352 a direct impact on the equivalent seismic magnitude. For instance, with a  
353 seismic efficiency of  $10^{-3}$  instead of  $10^{-4}$ , a meteoroid similar to the one  
354 which produced the Chicxulub crater in Mexico would be able to induce a  
355 seismic event of such a magnitude. Of course, the consequences would have  
356 been devastating.

357 We conclude that the surficial seismic events, including extra-terrestrial  
358 object impacts and explosions, are not efficient to make the inner-core oscil-  
359 late at the Slichter frequency with an amplitude large enough to be observed  
360 at the surface. The reason is the same as for earthquakes, i.e. the excitation  
361 amplitude is directly linked to the seismic magnitude and the radial eigen-  
362 functions of the Slichter mode are constant and close to zero in the mantle  
363 (Crossley, 1992; Rogister, 2003; Rosat, 2007).

## 364 **6. Conclusions and perspectives**

365 We have investigated the excitation of the translational free motion of the  
366 inner core by a pressure due to a flow in the outer core and acting at both the  
367 ICB and CMB, by a surface load, which can be associated to atmospheric or  
368 oceanic loading for instance, and by the collision between the Earth and a  
369 stellar object. Our conclusion is that the Slichter mode would be best excited  
370 by a pressure acting at the core boundaries at time-scales shorter than half  
371 the Slichter eigenperiod.

372 For the pressure source at the ICB and CMB and the loading source at the

373 surface, we have considered Gaussian functions of time. More complicated  
374 sources should be considered, in particular stochastic forces produced by  
375 some turbulent flow in the core or at the surface. The stochastic excitation,  
376 be it oceanic and atmospheric, of normal modes has been studied for instance  
377 by Tanimoto and Um (1999), Tanimoto (1999, 2007) and Webb (2007, 2008).  
378 However, the time scale for the Slichter mode is larger than for the other  
379 seismic normal modes, whose eigenperiod is shorter than 1 hour, so we should  
380 consider a theory different from the Kolmogorov theory of turbulence.

381 We have considered an analytic expression for the surface pressure as a  
382 source for the excitation of the Slichter mode. A more realistic approach  
383 should be based on actual atmospheric data from space correlation of world-  
384 wide barometers or from weather institutes (ECMWF, NCEP...), provided  
385 the data are available at a time resolution higher than the Slichter period.

386 **Appendix A. Evaluation of the time integral  $I(t)$  (Eq. 18)**

387 We evaluate the following integral:

$$I(t) = \int_{-\infty}^t e^{i\nu(t-t')} e^{-[\frac{t'-T_0}{\tau}]^2} dt'$$

388 We put  $b = \frac{t-T_0}{\tau}$  and introduce the variable  $x = \frac{t'-T_0}{\tau}$ .  $I(t)$  becomes:

$$I(t) = \tau \int_{-\infty}^b e^{i\nu\tau(b-x)} e^{-x^2} dx = \tau \int_{-\infty}^b e^{i\nu\tau b} e^{-x(x+i\nu\tau)} dx$$

389 We perform the change of variable  $y = x + i\frac{\nu\tau}{2}$ :

$$\begin{aligned} I(t) &= \tau e^{i\nu\tau b} \int_{-\infty}^{b+i\frac{\nu\tau}{2}} e^{-(y-i\frac{\nu\tau}{2})(y+i\frac{\nu\tau}{2})} dy \\ &= \tau e^{i\nu\tau b} e^{-\frac{\nu^2\tau^2}{4}} \int_{-\infty}^{b+i\frac{\nu\tau}{2}} e^{-y^2} dy \end{aligned}$$

390 The integral  $\frac{2}{\sqrt{\pi}} \int_z^{+\infty} e^{-y^2} dy$  is the complementary error function  $\text{erfc}(z) =$   
 391  $1 - \text{erf}(z)$ , where

$$\text{erf}(z) = \frac{2}{\sqrt{\pi}} \int_0^z e^{-y^2} dy. \quad (\text{A.1})$$

392 So the time integral  $I(t)$  is given by:

$$I(t) = \frac{\sqrt{\pi}}{2} \tau e^{i\nu(t-T_0)} e^{-\nu^2\tau^2/4} [1 + \text{erf}(\frac{t-T_0}{\tau} + i\frac{\nu\tau}{2})]$$

393 **References**

- 394 Aki, K. and Richards, P.G. (1980). Quantitative Seismology, Freeman, New  
395 York.
- 396 Alterman, Z., Jarosch, H. and Pekeris, L. (1959). Oscillations of the Earth,  
397 *Proc. Roy. Soc. Lond., Ser. A*, 252, 80-95.
- 398 Buffett B. A. (2010). Tidal dissipation and the strength of the Earth's internal  
399 magnetic field, *Nature*, 468, 952–954, doi:10.1038/nature09643
- 400 Buffett, B., Goertz, D.E. (1995). Magnetic damping of the translational os-  
401 cillations of the inner core, *Geophys. J. Int.*, 120, 103-110.
- 402 Chyba, C.F., Thomas, P.J. and Zahnle, K.J. (1993). The 1908 Tunguska  
403 explosion: Atmospheric disruption of a stony asteroid, *Nature*, 361, 40-44.
- 404 Collins, G.S., Melosh, H.J. and Marcus, R.A. (2005). Earth Impact Effects  
405 Program: A Web-based computer program for calculating the regional  
406 environmental consequences of a meteoroid impact on earth, *Meteoritics*  
407 *& Planetary Science*, 40 (6), 817-840.
- 408 Courtier, N., Ducarme, B., Goodkind, J., Hinderer, J., Imanishi, Y., Seama,  
409 N., Sun, H., Merriam, J., Bengert, B., Smylie, D.E. (2000). Global super-  
410 conducting gravimeter observations and the search for the translational  
411 modes of the inner core, *Phys. Earth Planet. Int.*, 117, 320.
- 412 Crossley, D.J. (1992). Eigensolutions and seismic excitation of the Slichter  
413 mode triplet for a fully rotating Earth model, *EOS*, 73, 60.

- 414 Crossley, D.J., Hinderer, J. and Legros, H. (1992). On the excitation, detec-  
415 tion and damping of core modes, *Phys. Earth Planet. Int.*, *68*, 97-116.
- 416 Dahlen, F.A. and Tromp, J. (1998). Theoretical Global Seismology, Prince-  
417 ton: Princeton Univ. Press., Princeton, NJ, 1025 pp.
- 418 Dziewonski, A.M., Anderson, D.L. (1981). Preliminary reference Earth model  
419 (PREM), *Phys. Earth Planet. Int.*, *25*, 297-356
- 420 Farrell, W.E. (1972). Deformation of the Earth by surface loads, *Rev. Geo-*  
421 *phys. Space Phys.*, *10*(3), 761-797.
- 422 Greff-Lefftz, M. and Legros, H. (1997). Some remarks about the degree-one  
423 deformation of the Earth, *Geophys. J. Int.*, *131*, 699-723.
- 424 Greff-Lefftz, M. and Legros, H. (2007). Fluid core dynamics and degree-one  
425 deformations: Slichter mode and geocentre motions, *Phys. Earth Planet.*  
426 *Int.*, *161*, 150-160.
- 427 Grinfeld, P. and Wisdom, J. (2010). The effect of phase transformations at  
428 the inner core boundary on the Slichter modes, *Phys. Earth Planet. Int.*,  
429 *178*, 3-4, 183-188.
- 430 Gubbins, D., Masters, G. and Nimmo, F. (2008). A thermochemical bound-  
431 ary layer at the base of Earth's outer core and independent estimate of  
432 core heat flux, *Geophys. J. Int.*, *174*, 1007-1018.
- 433 Guo, J.Y., Dierks, O., Neumeier, J. and Shum, C.K. (2007). A search for the  
434 Slichter modes in superconducting gravimeter records using a new method,  
435 *Geophys. J. Int.*, *168*, 507-517.

- 436 Hinderer, J., Crossley, D. and Jensen, O. (1995). A search for the Slichter  
437 triplet in superconducting gravimeter data, *Phys. Earth Planet. Int.*, *90*,  
438 183-195.
- 439 Hinderer, J. and Crossley, D. (2000). Time variations in gravity and infer-  
440 ences on the Earth's structure and dynamics, *Surv. Geophys.*, *21*, 1-45.
- 441 Jensen, O.G., Hinderer, J. and Crossley, D.J. (1995). Noise limitations in the  
442 core-mode band of superconducting gravimeter data, *Phys. Earth Planet.*  
443 *Int.*, *90*, 169-181.
- 444 Kanamori, H. and Cipar, J.J. (1974). Focal process of the great Chilean  
445 earthquake May 22, 1960, *Phys. Earth Planet. Int.*, *9*, 128-136.
- 446 Koper, K.D. and Dombrovskaya, M. (2005). Seismic properties of the inner  
447 core boundary from PKiKP/PcP amplitude ratios, *Earth Planet. Sci. Lett.*,  
448 *237*, 680-694.
- 449 Koper, K.D. and Pyle, M.L. (2004). Observations of PKiKP/PcP amplitude  
450 ratios and implications for Earth structure at the boundaries of the liquid  
451 core, *J. Geophys. Res.*, *109*, B03301.
- 452 Loper D. E. (2007). Turbulence and small-scale dynamics in the core, *In*  
453 Olson, P. (Ed.) Core dynamics, Vol. 2 Treatise on Geophysics, pp 187-  
454 206. (Ed. Schubert, G.), Elsevier: Amsterdam.
- 455 Masters, G. and Gubbins, D. (2003). On the resolution of the density within  
456 the Earth, *Phys. Earth Planet. Int.*, *140*, 159-167.



- 457 Melosh, H.J. (1981). Atmospheric breakup of terrestrial impactors. In *Multi-*  
458 *ring basins*, edited by Schultz P.H. and Merrill R.B. New York: Pergamon  
459 Press. pp. 29-35.
- 460 Melosh, H.J. (1989). *Impact cratering: A geologic process*. New York: Oxford  
461 University Press. 245 p.
- 462 Okubo, S. and Endo, T. (1986). Static spheroidal deformation of degree I.  
463 Consistency relation, stress solution and partials, *Geophys. J. R. Astron.*  
464 *Soc.*, *86*, 91-102.
- 465 Pagiatakis, S. D., Yin, H. and Abd El-Gelil, M. (2007). Least-squares self-  
466 coherency analysis of superconducting gravimeter records in search for the  
467 Slichter triplet, *Phys. Earth Planet. Int.*, *160*, 108-123.
- 468 Peng, Z.R. (1997). Effects of a mushy transition zone at the inner core bound-  
469 ary on the Slichter modes, *Geophys. J. Int.*, *131*, 607-617.
- 470 Rieutord, M. (2002). Slichter modes of the Earth revisited, *Phys. Earth*  
471 *Planet. Int.*, *131*, 269-278.
- 472 Rochester, M.G. and Peng Z.R. (1993): The Slichter modes of the rotating  
473 Earth: a test of the subseismic approximation, *Geophys. J. Int.*, *111*, 575-  
474 585.
- 475 Register, Y. (2003). Splitting of seismic free oscillations and of the Slichter  
476 triplet using the normal mode theory of a rotating, ellipsoidal earth, *Phys.*  
477 *Earth Planet. Int.*, *140*, 169-182.

- 478 Rogister Y. (2010). Multiple inner core wobbles in a simple Earth  
479 model with inviscid core, *Phys. Earth Planet. Int.*, 178, 8–15,  
480 doi:10.1016/j.pepi.2009.08.012.
- 481 Rogister Y. & Valette B. (2009). Influence of liquid core dynamics on ro-  
482 tational modes, *Geophys. J. Int.*, 176, 368–388, doi: 10.1111/j.1365-  
483 246X.2008.03996.x
- 484 Rosat, S., Hinderer, J., Crossley, D.J., Rivera, L. (2003). The search for the  
485 Slichter mode: comparison of noise levels of superconducting gravimeters  
486 and investigation of a stacking method. *Phys. Earth Planet. Int.*, 140 (13),  
487 183-202.
- 488 Rosat, S., Hinderer, J., Crossley, D.J., Boy, J.P. (2004). Performance of  
489 superconducting gravimeters from long-period seismology to tides, *J. of*  
490 *Geodyn.*, 38, 461-476.
- 491 Rosat, S., Rogister, Y., Crossley, D. et Hinderer, J. (2006). A search for the  
492 Slichter Triplet with Superconducting Gravimeters: Impact of the Density  
493 Jump at the Inner Core Boundary, *J. of Geodyn.*, 41, 296-306.
- 494 Rosat, S. (2007). Optimal Seismic Source Mechanisms to Excite the Slichter  
495 Mode. Int. Assoc. of Geod. Symposia, Dynamic Planet, Cairns (Australia),  
496 vol. 130, 571-577, Springer Berlin Heidelberg New York.
- 497 Rosat, S., Hinderer, J. (2011). Noise Levels of Superconducting Gravimeters:  
498 Updated Comparison and Time Stability, *Bull. Seism. Soc. Am.*, vol. 101,  
499 No. 3, doi: 10.1785/0120100217

- 500 Rosat, S., Saille, P. and Gegout, P. (2007). A wavelet-based detection and  
501 characterization of damped transient waves occurring in geophysical time-  
502 series: theory and application to the search for the translational oscillations  
503 of the inner core, *Geophys. J. Int.*, *171*, 55-70.
- 504 Schultz, P.H. and Gault, D.E. (1975). Seismic effects from major basin for-  
505 mation on the moon and Mercury, *The Moon*, *12*, 159-177.
- 506 Slichter, L.B. (1961). The fundamental free mode of the Earth's inner core,  
507 *Proc. Natl. Acad. Sci., USA*, *47*, 186-190.
- 508 Smith, M.L. (1976). Translational inner core oscillations of a rotating, slightly  
509 elliptical Earth, *J. Geophys. Res.*, *81* (17), 3055-3065.
- 510 Smylie, D.E. (1992). The inner core translational triplet and the density near  
511 Earth's centre, *Science*, *255*, 1678-1682.
- 512 Smylie, D.E., McMillan, D.G. (2000). The inner core as a dynamic viscome-  
513 ter, *Phys. Earth Planet. Int.*, *117*, 71-79.
- 514 Tanimoto, T. (1999). Excitation of normal modes by atmospheric turbulence:  
515 source of long-period seismic noise, *Geophys. J. Int.*, *136*, 395-402.
- 516 Tanimoto, T. (2007). Excitation of normal modes by non-linear interac-  
517 tion of ocean waves, *Geophys. J. Int.*, *168*(2), 571-582, doi:10.1111/j.1365-  
518 246X.2006.03240.x.
- 519 Tanimoto, T. and Um, J. (1999). Cause of continuous oscillations of the  
520 Earth, *J. Geophys. Res.*, *104*, 28723-28739.

- 521 Tkalčić, H., Kennett, B. L. N. and Cormier, V. F. (2009). On the inner-outer  
522 core density contrast from PKiKP/PcP amplitude ratios and uncertainties  
523 caused by seismic noise, *Geophys. J. Int.*, *179*, 425-443.
- 524 Tromp, J. and Mitrovica, J.X. (1999). Surface loading of a viscoelastic earth-  
525 I. General theory, *Geophys. J. Int.*, *137*, 847-855.
- 526 Valette B. (1989a). Spectre des vibrations propres d'un corps élastique, auto-  
527 gravitant, en rotation uniforme et contenant une partie fluide, *C. R. Acad.*  
528 *Sci. Paris*, **309**, Sér. I, 419-422.
- 529 Valette B. (1989b). Etude d'une classe de problèmes spectraux, *C. R. Acad.*  
530 *Sci. Paris*, **309**, Sér. I, 785-788.
- 531 Webb, S. C. (2007). The Earth's hum is driven by ocean waves over the  
532 continental shelves, *Nature*, *445*, 754-756, doi:10.1038/nature05536.
- 533 Webb, S. C. (2008). The Earth's hum: the excitation of Earth normal modes  
534 by ocean waves, *Geophys. J. Int.*, *174*, 542-566.

Table A.1: Some meteoroid impacts on the Earth continental crust and oceanic crust. The impact angle is supposed to be 45 degrees and the impact velocity is 20 km/s.

Location	Date (AD or My BP)	Diameter (m)	Density (kg/m <sup>3</sup> )	$M_w$	$\Delta g$ (nm/s <sup>2</sup> )
Tunguska Fireball Siberia	1908 AD	60	2700 (rock)	No impact	
Ries Crater Germany	$15.1 \pm 0.1$	1500	2700 (rock)	7.4	$3.9 \cdot 10^{-6}$
Rochechouart France	$214 \pm 8$	1500	3350 (stony-iron)	7.5	$4.9 \cdot 10^{-6}$
Chesapeake Bay USA	$35.5 \pm 0.3$	2300	2700 (rock)	7.8	$1.4 \cdot 10^{-5}$
Chicxulub Mexico	$64.98 \pm 0.05$	17500	2700 (rock)	9.6	$6.7 \cdot 10^{-3}$

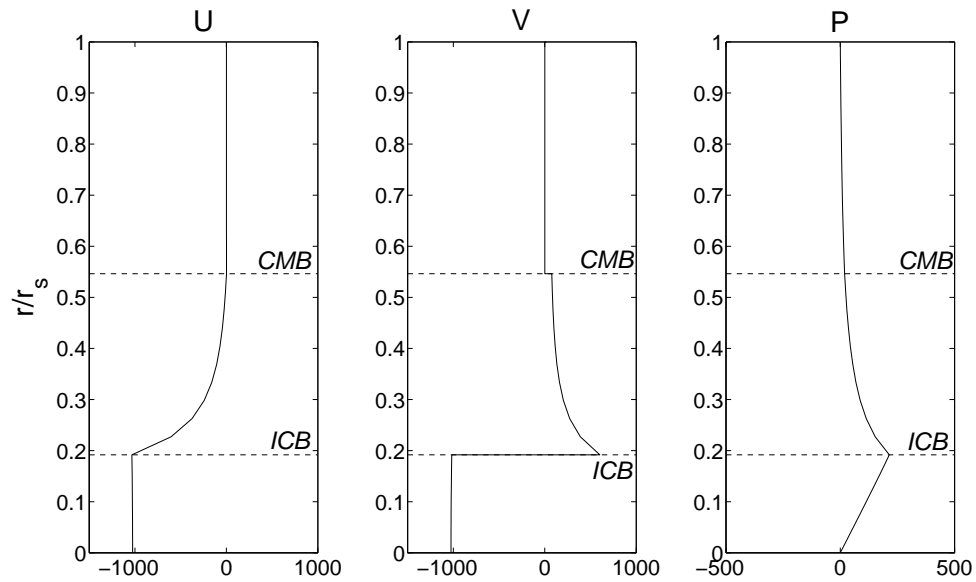


Figure A.1: Eigenfunctions of the Slichter mode  ${}_1S_1$  for the PREM model. The vertical axis is the radius normalized by the Earth's surface radius  $r_s$ .  $U$  and  $V$  are the radial dependence of the displacement given by Eq. (6).  $P$  is the perturbation of the gravitational potential. The normalization of the eigenfunctions is such that  $U(r_s) = 1$  m.

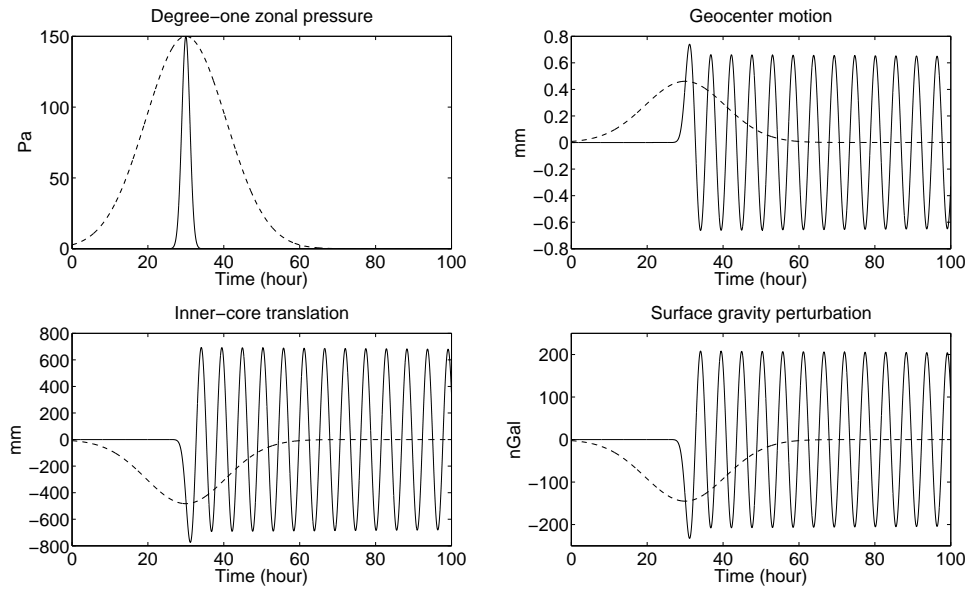


Figure A.2: Effects of the excitation of the Slichter mode by a fluid pressure acting at the CMB for two different excitation time-scales:  $\tau = 1.5$  h (solid line) and  $\tau = 15$  h (dashed line). This figure is similar to Fig. 3 of Greff-Lefftz and Legros (2007) but we have applied a Green tensor formalism to the PREM model. (a) Degree-one zonal pressure; (b) geocentre motion; (c) inner-core translation; (d) surface gravity perturbation.

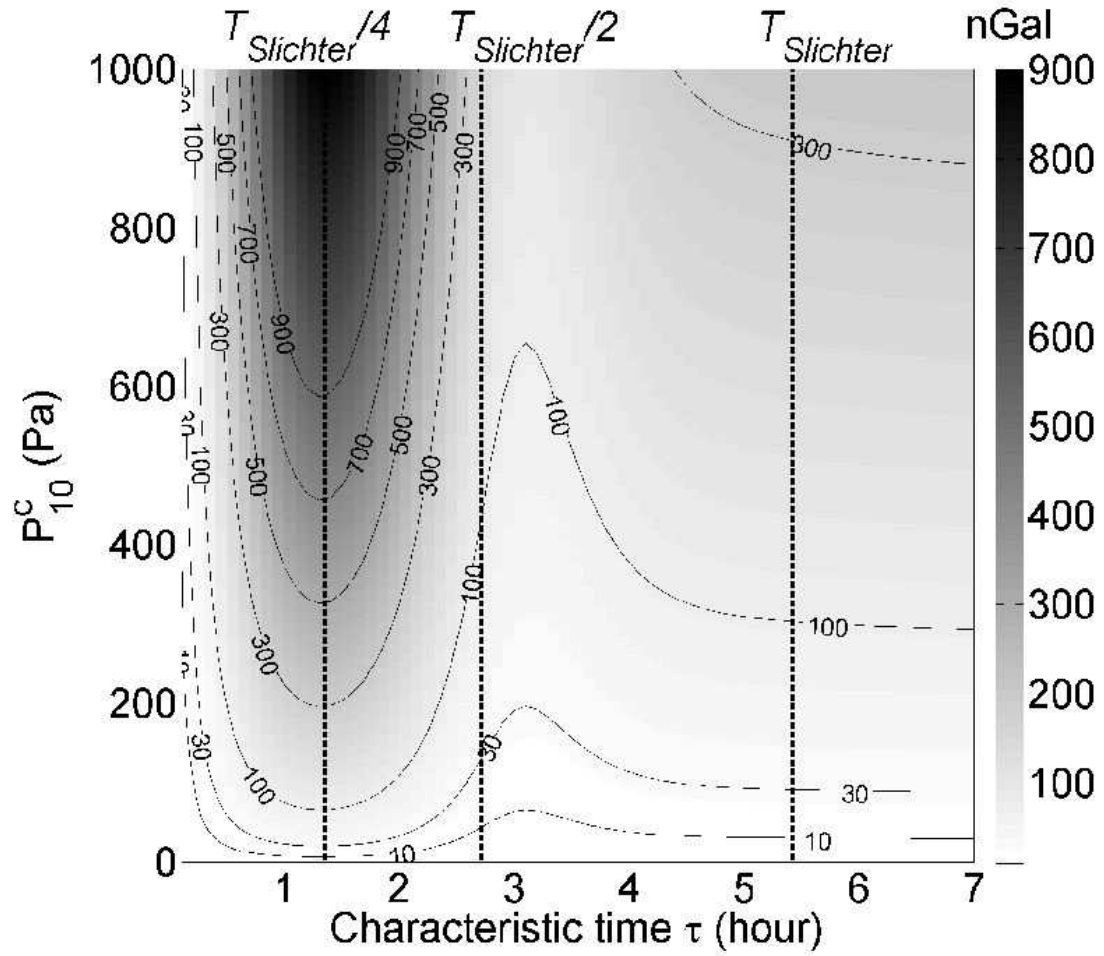


Figure A.3: Surface gravity perturbation induced by the Slichter mode excited by a fluid pressure acting at the CMB for different excitation time-scales and various zonal pressure amplitudes. The vertical dotted lines correspond to one fourth of the Slichter period, one half of the Slichter period and the Slichter period.



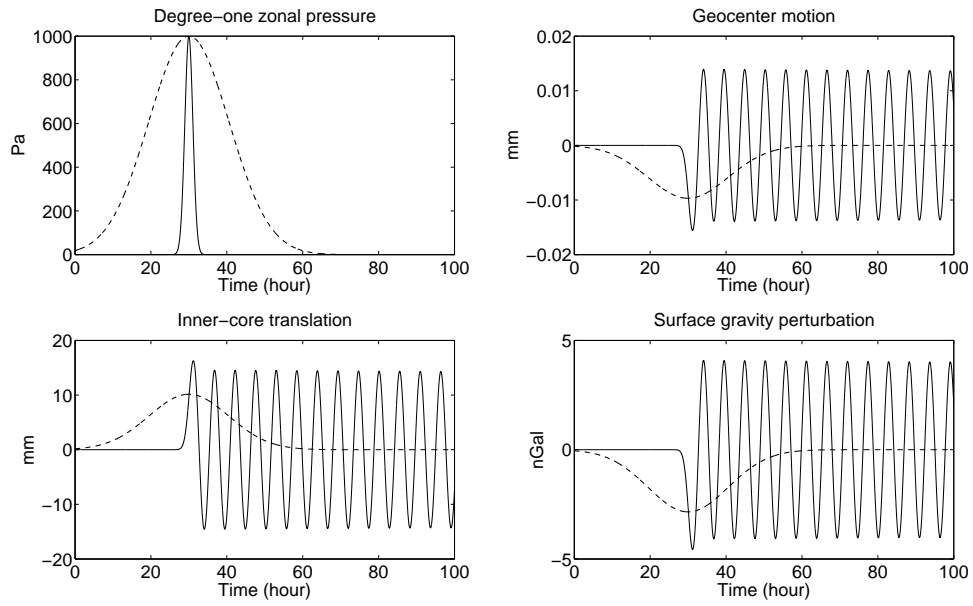


Figure A.4: Resulting effects of the excitation of the Slichter mode by a zonal surface load  $\sigma(t) = \sigma_0 e^{-[\frac{t-T_0}{\tau}]^2}$  for two different excitation time-scales:  $\tau = 1.5$  h (solid line) and  $\tau = 15$  h (dashed line). (a) Degree-one zonal pressure effect; (b) geocentre motion; (c) inner-core translation; (d) surface gravity perturbation.

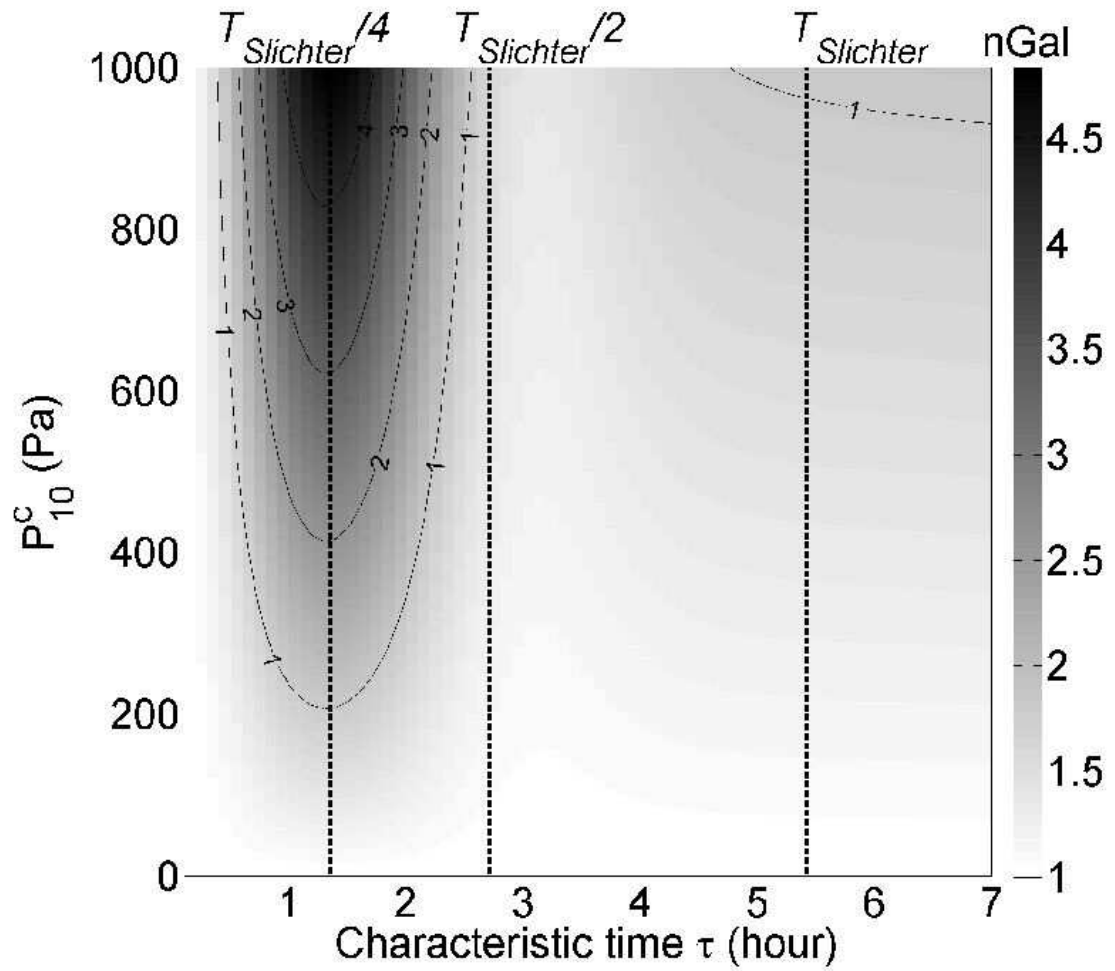


Figure A.5: Surface gravity perturbation induced by the Slichter mode excited by a surface load for different excitation time-scales and various zonal pressure amplitudes.

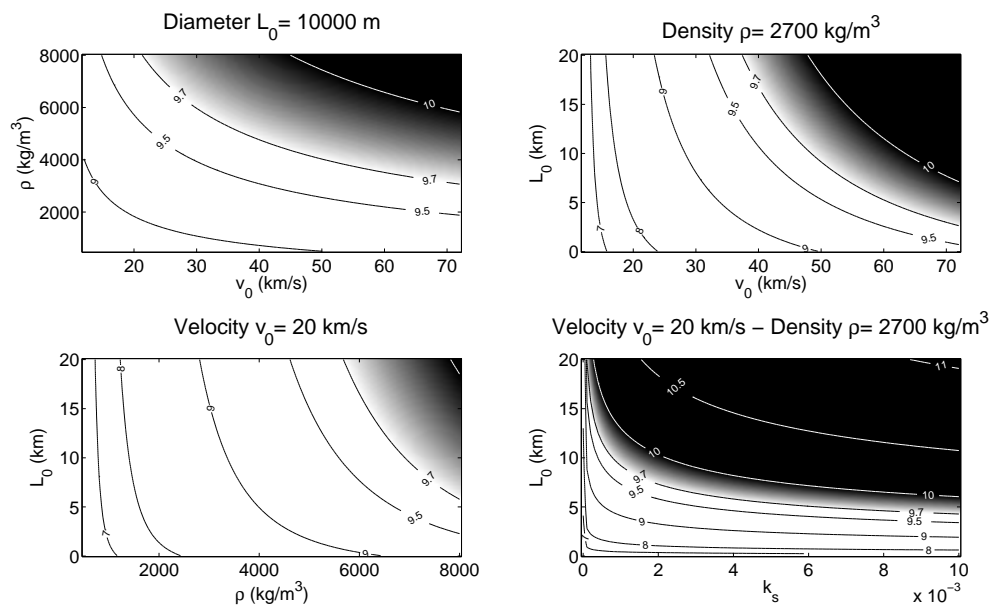


Figure A.6: Seismic magnitude as a function of the impactor parameters and seismic efficiency  $k_s$ . The shaded area corresponds to moment magnitudes larger than 9.7, i.e. to induced surface gravity perturbation larger than 1 nGal.

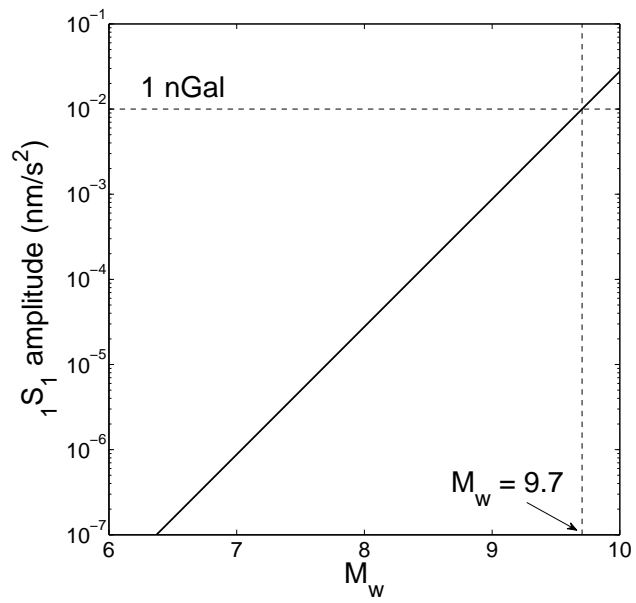


Figure A.7: Surface gravity perturbation induced by the Slichter mode as a function of the moment magnitude of a superficial energy release (explosion or object impact).